Journal of Alloys and Compounds 509 (2011) 366–371

Contents lists available at ScienceDirect

Journal of Alloys and Compounds

journal homepage: www.elsevier.com/locate/jallcom

The influence of Sc/Lu ratio on the phase transformation and luminescence of cerium-doped lutetium scandium orthoborate solid solutions

Yuntao Wu, Dongzhou Ding, Shangke Pan, Fan Yang, Guohao Ren*

Shanghai Institute of Ceramics, Chinese Academy of Sciences, No. 215 Chengbei Road, Jiading, Shanghai 201800, PR China

ARTICLE INFO

Article history:
Received 30 June 2010
Received in revised form 1 September 2010
Accepted 3 September 2010
Available online 21 September 2010

Keywords:
Phase transformation
Lutetium scandium orthoborate
Solid solutions
Luminescence

ABSTRACT

The dependence of structural characteristics of cerium-doped lutetium scandium orthoborate $(Lu_{1-x}Sc_x)BO_3$:Ce solid solutions on Sc/Lu ratio was investigated. It was found that the calcite phase of $LuBO_3$ can be stabilized up to 1550 °C at least when the $n(Sc)/n(Lu+Sc)$ ratio was ≥10 at.%. The closed correlations between Sc^{3+} or Ce^{3+} molar ratio in the host and luminescence mechanism were discussed in detail. Based on the requirements of steady phase structure, better luminescence efficiency and higher density, the reasonable $n(Sc)/n(Lu+Sc)$ and $n(Ce)/n(RE)$ ratio should be in the range of 30–50 at.% and 0.3–0.5 at.%, respectively. A modified composition, $(Lu_{0.5}Sc_{0.5})_{0.995}Ce_{0.005}BO_3$ solid solution, was selected to grow single crystal. Its X-ray excited luminescence intensity can be as high as about 27% of LYSO:Ce standard crystal and the effective lifetime is round 20.1 ns. Hence, the cerium-doped lutetium scandium orthoborate crystal is a promising scintillator for X-ray detection or γ-ray detection.

1. Introduction

Scintillation materials are widely used in high-energy physics, nuclear medical imaging and security inspection. Nowadays, many researchers are devoting to researching and optimizing the existing scintillation crystals [1–4], and also developing new scintillators such as $Y_2Si_2O_7$:Ce, $Gd_2Si_2O_7$:Ce and $MgWO_4$ [5–7]. Nevertheless, there are still many novel crystals deserved to be developed. The cerium activated lutetium orthoborate is one of the excellent sinctillators when the best performance is achieved by a compromise between characteristics, i.e. high density, high light output, and fast response time [8–10], which can be used for high-energy physics and medical application. In recent years, increased interest of researchers has been devoted to submicron and nanodimensional crystalline powders of cerium activated lutetium orthoborate, which is expected to be good prospect for the creation of effective scintillation films and composites [11–15].

However, because the phase transformation [16] occurred at 1310 °C (at atmospheric pressure), it is very difficult to obtain $LuBO_3$ single crystal from its melt. Therefore, there are few literatures about its scintillation characteristics. Moreover, according to our present research result, the phase transition behavior of $LuBO_3$ is more complicated than that reported previously. Hence, growth of the crystal has always been regarded as impossible, unless its phase transformation problem can be solved. Nedelec et al. [17] once proposed that doping with rare earth ions can prevent the phase transformation in $LuBO_3$, but so far the specific rare earth ions that can stabilize the calcite phase or vaterite phase were not obtained. Just when $LuBO_3$ crystal research got into difficulties, Sc^{3+} was reported to be a phase stabilizing ion and $Lu_{0.9}Sc_{0.1}BO_3$:Ce single crystals were successfully obtained, even though the relative light yield of the crystal was less than 60% of BGO [18]. However, to our knowledge, the mechanisms of Sc/Lu ratio on the structural stability and luminescence characteristic in $Lu_{1-x}Sc_xBO_3$:Ce materials are still unknown, which is highly important to further $Lu_{1-x}Sc_xBO_3$:Ce crystal growth and scintillation characteristics research.

Hence, the aim of this study is to investigate the structural stability and luminescence properties of cerium-doped lutetium scandium orthoborate solid solutions at different Sc/Lu ratios and Ce^{3+} concentrations in the host, and explore the optimum compositions with steady phase structure and better luminescence efficiency to guide the growth of $Lu_{1-x}Sc_xBO_3$:Ce crystals. Under the guidance of reasonable composition selection, the $(Lu_{0.5}Sc_{0.5})_{0.995}Ce_{0.005}BO_3$ crystal was successfully obtained by Czochralski method and its luminescence properties were also investigated.

2. Experimental

Cerium-doped lutetium scandium orthoborate solid solution powders were synthesized in the muffle furnace by solid state reaction method. The starting materials are Lu_2O_3, Sc_2O_3, H_3BO_3, CeO_2 powder with 99.99% purity. The powders were weighed according to the stoichiometric ratio of two series samples, i.e. $(Lu_{1-x}Sc_x)_{0.995}Ce_{0.005}BO_3$ (x = 0–1; the interval is 0.1) and $Lu_{0.7-x}Sc_{0.3}Ce_xBO_3$ (x = 0.001, 0.003, 0.005, 0.01 and 0.03) except for H_3BO_3 which was 5 wt% rich due

* Corresponding author. Tel.: +86 21 69987740; fax: +86 21 59927184.
E-mail address: rgh@mail.sic.ac.cn (G. Ren).

0925-8388/$ – see front matter © 2010 Elsevier B.V. All rights reserved.
doi:10.1016/j.jallcom.2010.09.027

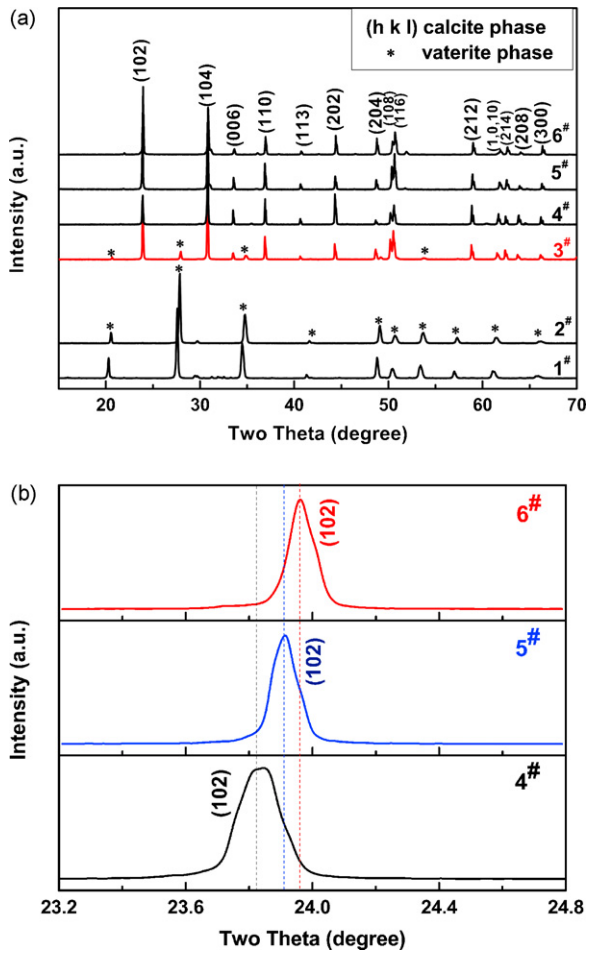

Fig. 1. XRD patterns of $(Lu_{1-x}Sc_x)_{0.995}Ce_{0.005}BO_3$ solid solutions (a); expanded view of the 2θ diffraction peaks between 23° and 25° (b).

to vaporization loss during high-temperature synthesized, and then mixed for 1 h, respectively. The mixture was loaded in alumina crucibles, sintered in the furnace in atmosphere at 1550 °C for 15 h, and evenly cooled down to room temperature within 12 h, respectively.

$(Lu_{0.5}Sc_{0.5})_{0.995}Ce_{0.005}BO_3$ single crystal was grown by Czochralski method. Lu_2O_3, Sc_2O_3, CeO_2 and H_3BO_3 with purity of 4N were weighed in composition formula $(Lu_{0.5}Sc_{0.5})_{0.995}Ce_{0.005}BO_3$ except for H_3BO_3 which was 5 wt% rich due to vaporization loss during crystal growth. Mixtures of raw materials were calcined at 1200 °C for 15 h to form polycrystals and then charged into an iridium crucible of dimensions $\varnothing 60 \times 40\,mm^3$. Crystal growth was carried out in argon atmosphere with 2 mm/h pulling rate and 10 rpm rotating rate. The as-grown crystals were cut into small specimen of approximate dimensions 2 mm × 2 mm × 2 mm, which are clear and no macroscopic imperfections, such as veils, voids or inclusions. A commercial $(Lu_{0.8}Y_{0.2})_{1.995}Ce_{0.005}SiO_5$ (LYSO:Ce) single crystal with the same size supplied by SICCAS was used as a standard to compare the luminescence intensity of $(Lu_{0.5}Sc_{0.5})_{0.995}Ce_{0.005}BO_3$ crystal.

The structures of the obtained crystals were determined by Rigaku D\max-2550 V (scanning rate = 2.4°/min at 40 kV and 50 mA) where Cu Kα was used as incident X-ray (XRD measurement). Phase characterization was carried out using Jade software and lattice parameters were determined by performing a least square regression on the 2θ-values for the 10 most intense peaks on the calibrated patterns. The photoluminescence spectrum (PL) and fluorescence lifetime spectrum were recorded on the Perkin-Elmer LS50B and FLS-920 spectrofluorometer, respectively. The X-ray excited emission spectra (XEL) were conducted on an X-ray Excited Luminescence Spectrometer, assembled at Shanghai Institute of Ceramics. The X-ray tube was operated at the condition of $V = 60$ kV, $I = 2$ mA. The powders were pressed into round tablets with smooth surface before luminescence measurements.

3. Results and discussion

The XRD patterns of $(Lu_{1-x}Sc_x)_{0.995}Ce_{0.005}BO_3$ polycrystals are shown in Fig. 1. The phase composition of the samples obtained from different Sc/Lu ratios and experimental conditions are presented in Table 1. It is observed from the figure that three phases can be identified from the samples with different Sc^{3+} doping concentrations. For the 1# and 2# samples, all the diffraction peaks can be well assigned to the $LuBO_3$ vaterite phase (PDF# 13-0481). While, vaterite and calcite phase coexist in the 3# sample. All of the diffraction peaks of the 4#–6# samples can be well assigned to a calcite phase structure with the characteristic diffraction peaks of lutetium orthoborate ($LuBO_3$, PDF# 72-1053) just with accordant movement to higher angle. Except the phases mentioned above, no other phases, such as Sc_2O_3, Lu_3BO_6 can be identified, which reveals that doping Sc^{3+} at different concentrations does not induce a new phase, and the Sc^{3+} ions are likely to enter $LuBO_3$ crystal lattice to substitute Lu^{3+} sites. Based on the difference of the main diffraction peak (1 0 2) of the 4#–6# samples, which is shown in Fig. 1(b), it is observed that the diffraction peak of (1 0 2) shifts obviously toward higher angle with increasing of the Sc^{3+} doping concentration. According to the Bragg equation, the shift of diffraction peaks toward higher angle reveals that the cell parameters of samples could continuously decrease with the increase of Sc^{3+} content. As the ion radius of Sc^{3+} (74.5 pm) is smaller than Lu^{3+} (86.1 pm), the lattice constant of calcite phase of Sc^{3+} doped $LuBO_3$:Ce could be undoubtedly reduced. It is also observed that when the $n(Sc)/n(Sc + Lu)$ ratio is ≥10 at.%, the calcite phase solid solutions can be stabilized at high temperature up to 1550 °C at least.

The role of Sc^{3+} ions on the phase stability of calcite may be related with its smaller ionic radius. According to Pauling's rule [19], the coordination number of cation in crystal structure corresponds to the radius ratio of cation to anion. When the ratio varies among 1–0.732 and 0.732–0.414, the coordination numbers of cations are 8 and 6, respectively. The $R(Lu^{3+})/R(O^{2-})$ ratio in $LuBO_3$ is calculated to be 0.688, therefore the coordination number of Lu^{3+} in a stable structure should be 6. Obviously the radius of Lu^{3+} is too small to keep $LuBO_3$ with vaterite structure (eightfold coordination). Contrarily, small cationic radius is beneficial to $LuBO_3$ with calcite phase (sixfold coordination). Hence, by doping appropriate type of cation, the $LuBO_3$ crystal with calcite phase could be grown from the melt, similar to the way of doping Y^{3+} to stabilize the LuAP phase in $LuAlO_3$ crystal materials [20]. In addition, $ScBO_3$ not only has identical crystal structure with calcite phase of $LuBO_3$ [21] but also is a congruent compound [22].

The influence of the Sc/Lu ratio on the luminescence properties of $(Lu_{1-x}Sc_x)_{0.995}Ce_{0.005}BO_3$ solid solutions was characterized. Fig. 2 shows the photoluminescence spectra of $(Lu_{1-x}Sc_x)_{0.995}Ce_{0.005}BO_3$ ($x \geq 0.1$) solid solutions. All spectra were monitored at their most effective excitation and emission wavelengths. It is observed that the typical Ce^{3+} emission band of $(Lu_{1-x}Sc_x)_{0.995}Ce_{0.005}BO_3$ corresponding to the lowest $5d \rightarrow 4f$ ($^2F_{5/2}$ and $^2F_{7/2}$) transitions locates in the range between 340 nm and 480 nm, and the Ce^{3+} excitation band locates between 260 nm and 360 nm. A consistent redshift with the increase of Sc ions content can be both observed in the excitation and emission spectra. The cause will be discussed later.

Fig. 3(a) shows the XEL spectra of $(Lu_{1-x}Sc_x)_{0.995}Ce_{0.005}BO_3$ solid solutions with calcite structure. The Ce^{3+} emission band of $(Lu_{1-x}Sc_x)_{0.995}Ce_{0.005}BO_3$ ($x \geq 0.1$) in XEL spectra is similar with the photoluminescence spectra, which is considerably different from that of $LuBO_3$:Ce vaterite phase ($x = 0$) sample due to structure discrepancy. Apart from this, two interesting phenomena deserved to be noticed.

The first one is that the Ce^{3+} luminescence band of $(Lu_{1-x}Sc_x)_{0.995}Ce_{0.005}BO_3$ gradually shifts toward longer wavelength as Sc content increases. As we known, the 5d configuration of Ce^{3+} ions is split into five different crystal-field components at most and is shifted to deep levels in the band gap comparing to Ce^{3+} as a free ion. The total shift is defined as $D(A)$ and can be written as

Table 1
Phase composition and experimental condition.

Sample number	Nominal composition	Phase composition	Experimental condition
1#	100 at.% $LuBO_3$	Vaterite	Calcined at 1550 °C for 15 h, and then cooled to room temperature within 12 h
2#	95 at.% $LuBO_3$ + 5 at.% $ScBO_3$	Vaterite	
3#	93 at.% $LuBO_3$ + 7 at.% $ScBO_3$	Vaterite + calcite	
4#	90 at.% $LuBO_3$ + 10 at.% $ScBO_3$	Calcite	
5#	80 at.% $LuBO_3$ + 20 at.% $ScBO_3$	Calcite	
6#	70 at.% $LuBO_3$ + 30 at.% $ScBO_3$	Calcite	

[23]:

$$D(A) = \varepsilon_c(A) + \frac{\varepsilon_{cfs}(A)}{r(A)} - 1890\,\mathrm{cm}^{-1} \quad (1)$$

In the above equation, the centroid shift $\varepsilon_c(A)$ is the lowering of the average (centroid) of the five 5d levels. The crystal-field splitting $\varepsilon_{cfs}(A)$ is defined as the energy difference between the lowest and highest 5d level. A fraction $1/r(A)$ contributes to the redshift. The value of $r(A)$ is usually between 1.7 and 2.4. According to the results reported by Dorenbos [24], it is believed that provided that polyhedral shape remains constant, crystal-field splitting $\varepsilon_{cfs}(A)$ depends on the average distance to the ligands; large cations increase the polarizability of the anions and thus increase the centroid shift $\varepsilon_c(A)$. Due to the longer Lu–O distance and larger Lu^{3+} ionic radius in calcite phase of $LuBO_3$, its $D(A)$ is smaller than that of $ScBO_3$. It also means that lowest energy Ce^{3+} $5d \rightarrow 4f$ emission bands of $ScBO_3$ have redshift comparing to that of calcite phase of $LuBO_3$. Therefore, it is reasonable to assume that, for $Lu_{1-x}Sc_xCe_{0.005}BO_3$ solid solution, with the increase of Sc^{3+} content, the lowest 5d excitation shifts to lower energies and in turn there should be a continuous redshift of the lowest energy Ce^{3+} $5d \rightarrow 4f$ emission band. These expectations are fully in accord with the features appeared in Fig. 3(a).

The second one is the difference spectrum shown in the inset of Fig. 3(a). It is observed that with the increase of Sc content, the intensity of luminescence band corresponding to the $4f^05d^1 \rightarrow 4f^1(^2F_{7/2})$ transition increases, whereas the intensity of luminescence band corresponding to the $4f^05d^1 \rightarrow 4f^1(^2F_{5/2})$ transition decreases. However, the cause is still unknown.

The intensity of luminescence excited by high-energy ray, i.e. X-ray, γ-ray is usually regarded as an important standard to evaluate the luminescence efficiency of scintillation samples. Fig. 3(b) shows X-ray excited emission spectra of $(Lu_{1-x}Sc_x)_{0.995}Ce_{0.005}BO_3$ and the dependence of integrated intensity on the $n(Sc)/n(Sc+Lu)$ ratio. As the $n(Sc)/n(Sc+Lu)$ ratio increases from 10 at.% to 40 at.%, the luminescence efficiency of Ce^{3+} increases considerably, and then decreases as the Sc^{3+} concentration level increases further. The optimal luminescence efficiency is achieved when the $n(Sc)/n(Sc+Lu)$ ratio is round 40 at.%.

Fig. 4(a) shows the XEL spectra of $Lu_{0.7-x}Sc_{0.3}Ce_xBO_3$ solid solutions and PL spectra of $Lu_{0.695}Sc_{0.3}Ce_{0.005}BO_3$ solid solution. The inset is the self-trapped excitons (STE) emission spectra of $Lu_{0.7-x}Sc_{0.3}Ce_xBO_3$ solid solutions. It is observed that the wavelengths of Ce^{3+} emission peaks corresponding to the lowest $5d \rightarrow 4f$ ($^2F_{5/2}$ and $^2F_{7/2}$) transitions in the XEL spectra are almost identical to PL emission spectra. Note that the high-energy emission ($4f^05d^1 \rightarrow 4f^1(^2F_{5/2})$) is truncated on the short wavelength side and the intensity ratio of the two emission bands varies with the increase of Ce^{3+} content. This indicates the presence of self-absorption due to the high concentration of Ce^{3+}. It is also observed that the broad emission band in 200–325 nm range peaking at 269 nm is distinctly different from the observed Ce^{3+} emission for the low Ce^{3+} concentration samples, i.e. 0.1 at.%, 0.3 at.%, and 0.5 at.%. This broad emission band can be ascribed to the self-trapped exciton (STE) emission [25]. Observed from the PL excitation spectrum and XEL spectra, the Ce^{3+} ion excitation state of the lowest crystal field component of the 5d energy level does not overlap well with the STE emission band, and a good overlap can be expected with the higher-lying 5d levels of Ce^{3+}. And the luminescence intensity of STE dramatically decreases with the increase of Ce^{3+} concentration. Hence, it is suggested that the efficient energy transfer from the STE to Ce^{3+} could takes place according to the Forster–Dexter dipole–dipole energy transfer theory [26]. In addition, Feofilov et al. [25] reported an energy transfer from

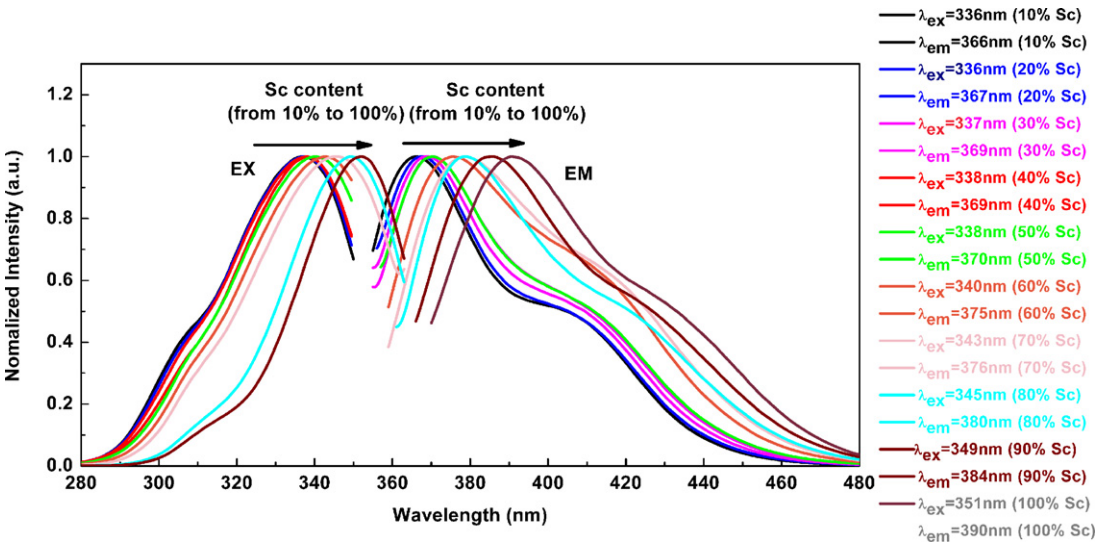

Fig. 2. Photoluminescence spectra of the $(Lu_xSc_{1-x})_{0.995}Ce_{0.005}BO_3$ solid solutions. All spectra were monitored at their most effective excitation and emission wavelengths.

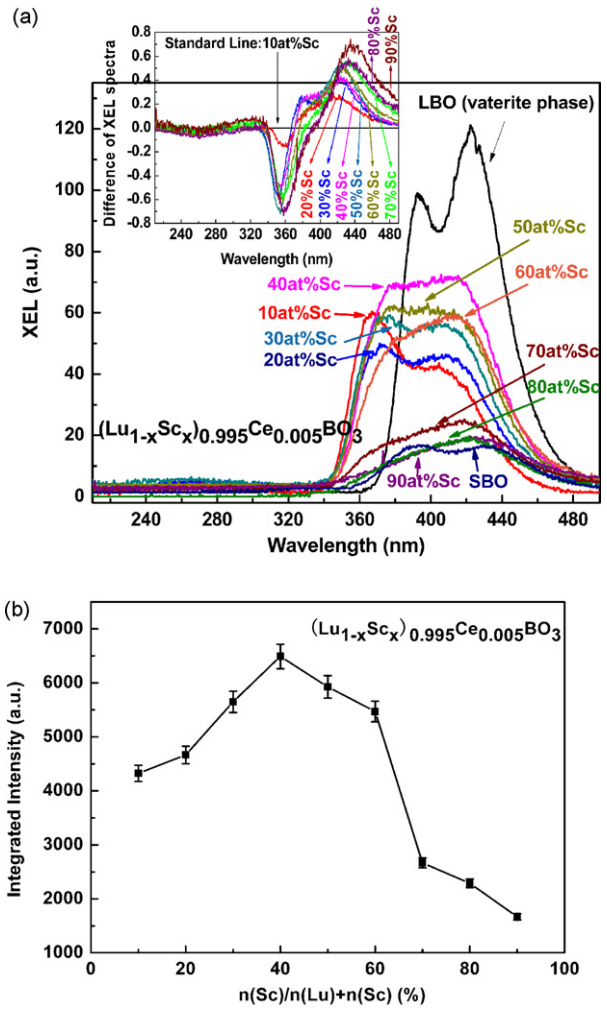

Fig. 3. XEL spectra of the $(Lu_{1-x}Sc_x)_{0.995}Ce_{0.005}BO_3$ solid solutions (a); dependence of integrated luminescence intensity of $(Lu_{1-x}Sc_x)_{0.995}Ce_{0.005}BO_3$ solid solutions on the content of n(Sc)/n(Sc + Lu) under X-ray excited (b).

self-trapped excitons (STE) to the Ce^{3+} ion in $ScBO_3$. Dependence of integrated intensity of $Lu_{0.7-x}Sc_{0.3}Ce_xBO_3$ solid solution polycrystals on n(Ce)/n(RE) ratio is shown in Fig. 4(b). It is observed that the integrated intensity of $Lu_{0.7-x}Sc_{0.3}Ce_xBO_3$ solid solution polycrystals increases with the content of Ce^{3+}, and reaches maximum at 0.3 at.%, and then decreases due to the concentration quenching effect. Hence, the preferable Ce^{3+} content is about 0.3 at.%.

According to above results, it is believed that the optimum n(Sc)/n(Lu + Sc) and n(Ce)/n(RE) ratio should be in the range of 30–50 at.% and 0.3–0.5 at.%, respectively. Therefore, $(Lu_{0.5}Sc_{0.5})_{0.995}Ce_{0.005}BO_3$ composition is chosen to grow single crystal and the grown ingot is shown in Fig. 5(a). Its X-ray diffraction pattern is displayed in Fig. 5(b). All diffraction peaks can be well assigned to the calcite phase structure with the characteristic of lutetium orthoborate ($LuBO_3$, PDF# 72-1053) and scandium orthoborate ($ScBO_3$, PDF# 79-0079), just with differences in the diffraction peak angle. It demonstrates that the as-grown $(Lu_{0.5}Sc_{0.5})_{0.995}Ce_{0.005}BO_3$ crystal is in the form of solid solution with the hexagonal structure of $R\bar{3}c$ space group, which corroborates that doping smaller radius ion Sc^{3+} can stabilize the calcite phase of $LuBO_3$. The obtained lattice parameters of $(Lu_{0.5}Sc_{0.5})_{0.995}Ce_{0.005}BO_3$ crystal are, $a = b = 4.859$ Å, $c = 15.893$ Å, respectively. Compared with lattice parameters of $LuBO_3$ calcite phase $a = b = 4.913$ Å, $c = 16.214$ Å and $ScBO_3$ calcite phase $a = b = 4.748$ Å, $c = 15.260$ Å, the lattice parameters of the

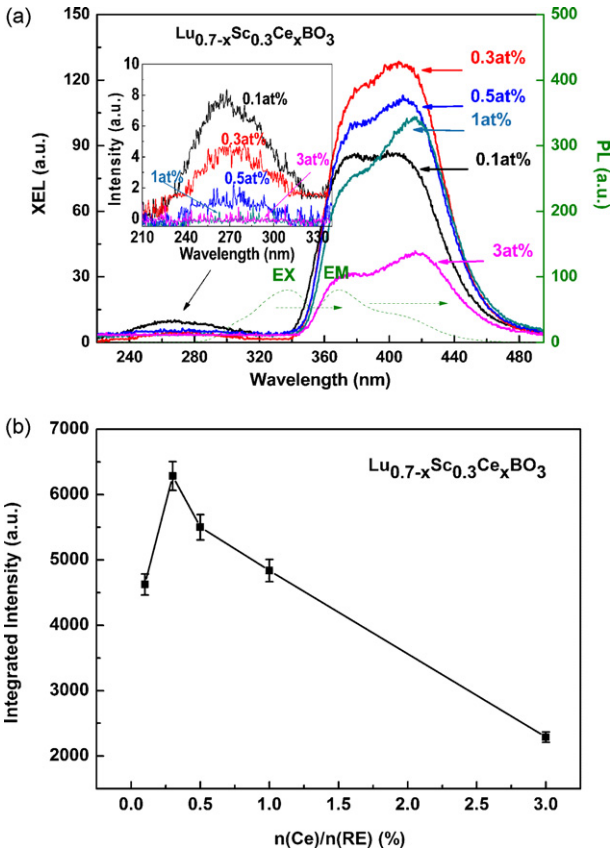

Fig. 4. XEL spectra of the $Lu_{0.7-x}Sc_{0.3}Ce_xBO_3$ solid solutions (a), inset is the STE emission spectra of $Lu_{0.7-x}Sc_{0.3}Ce_xBO_3$ solid solutions; dependence of integrated luminescence intensity of $Lu_{0.7-x}Sc_{0.3}Ce_xBO_3$ on the content of n(Ce)/n(RE) under X-ray excited (b).

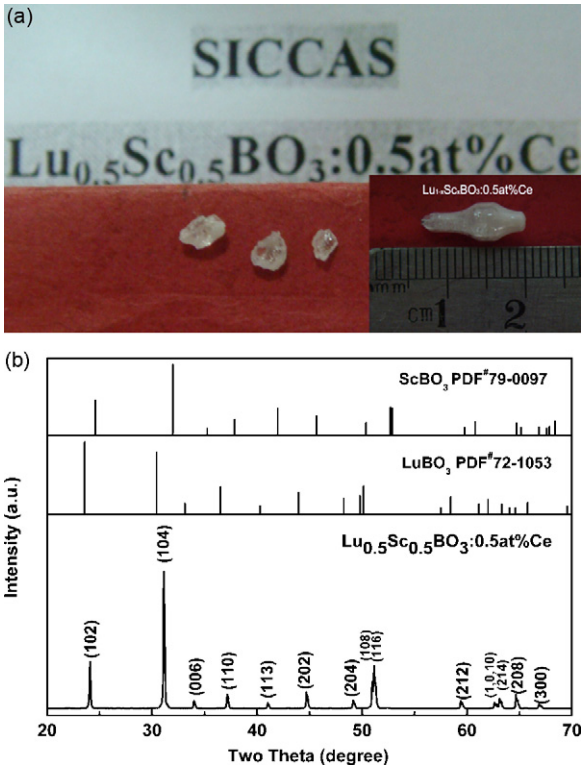

Fig. 5. Photo of $(Lu_{0.5}Sc_{0.5})_{0.995}Ce_{0.005}BO_3$ single crystal (a); inset is the $(Lu_{1-x}Sc_x)_{0.995}Ce_{0.005}BO_3$ single crystal; XRD pattern of $(Lu_{0.5}Sc_{0.5})_{0.995}Ce_{0.005}BO_3$ single crystal (b).

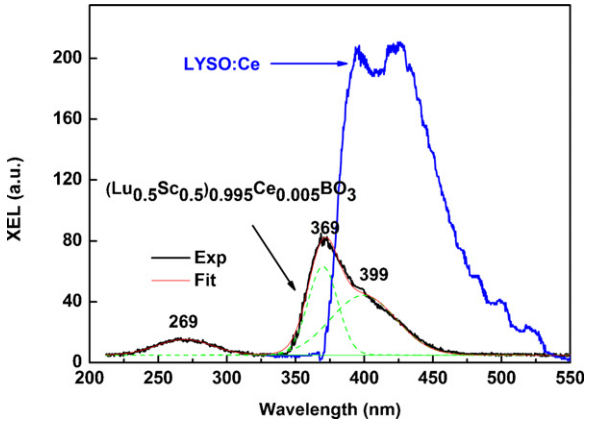

Fig. 6. X-ray stimulated luminescence spectra of $(Lu_{0.5}Sc_{0.5})_{0.995}Ce_{0.005}BO_3$ single crystal comparing to commercial LYSO:Ce single crystal.

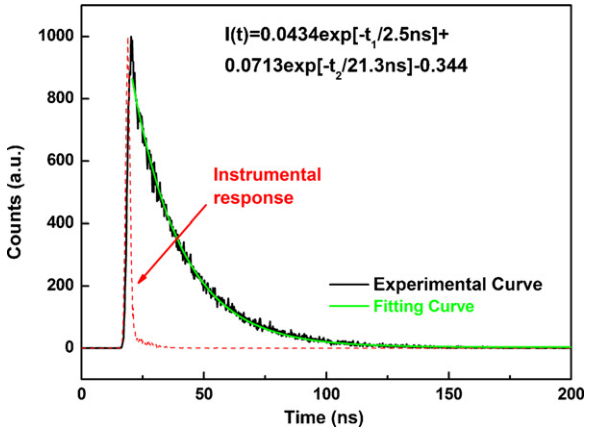

Fig. 7. Decay curve of $(Lu_{0.5}Sc_{0.5})_{0.995}Ce_{0.005}BO_3$ single crystal monitoring the Ce^{3+} emission at 340 nm for excitation and 369 nm for emission.

$(Lu_{0.5}Sc_{0.5})_{0.995}Ce_{0.005}BO_3$ are not completely satisfied with the Vegard law [27]. This is because Vegard's law [28] is an approximation applicable to ideal solutions only when the difference in atomic radii or lattice parameters of the two components forming a solid solution is small (less than 5%). Herein, the difference of lattice constant c between $LuBO_3$ and $ScBO_3$ is over 6% and the difference in atomic radius of Lu and Sc is over 7%.

The X-ray excited luminescence spectra of both $(Lu_{0.5}Sc_{0.5})_{0.995}Ce_{0.005}BO_3$ crystal and LYSO:Ce crystal measured at room temperature are plotted in Fig. 6. $(Lu_{0.5}Sc_{0.5})_{0.995}Ce_{0.005}BO_3$ crystal sample shows a double peaked emission band with maxima at 369 and 399 nm. These bands, similar to the PL spectrum shown in Fig. 2, are attributed to the $4f^05d^1$–$4f^1(^2F_{5/2})$ and $4f^05d^1$–$4f^1(^2F_{7/2})$ transition of Ce^{3+} ions, respectively. And the self-trapped excitons (STE) band locates in the range from 225 nm to 325 nm peaking at 269 nm. Note that the STE luminescence of $(Lu_{0.5}Sc_{0.5})_{0.995}Ce_{0.005}BO_3$ solid solution crystal is more distinct than that of $(Lu_{0.5}Sc_{0.5})_{0.995}Ce_{0.005}BO_3$ solid solution powders. It is caused by the extremely low Ce^{3+} concentration in crystal due to small segregation coefficient [18], which directly lowers nonradiative energy transfer probability from STE to Ce^{3+} ion.

The relative light yield of $(Lu_{0.5}Sc_{0.5})_{0.995}Ce_{0.005}BO_3$ (LSBO:Ce) crystal is evaluated by the ratio of the integrated intensity ($I_{LSBO:Ce}$) with that of a LYSO:Ce ($I_{LYSO:Ce}$) standard sample. The equation is as follow:

$$\alpha_{ph} = \frac{\int I_{LSBO:Ce}(\lambda)d\lambda_{LSBO:Ce}}{\int I_{LYSO:Ce}(\lambda)d\lambda_{LYSO:Ce}} \quad (2)$$

We obtain that the relative light yield of $(Lu_{0.5}Sc_{0.5})_{0.995}Ce_{0.005}BO_3$ crystal (Ce^{3+} emission) is round 27% of LYSO:Ce.

The decay curve of $(Lu_{0.5}Sc_{0.5})_{0.995}Ce_{0.005}BO_3$ crystal is shown in Fig. 7. The monitoring excitation and emission wavelengths are fixed at 340 and 369 nm, respectively, which are the most effective excitation and emission wavelengths for the sample. Using double exponential decay kinetics fitting, good fitting curves are obtained with small weighted residuals. The double-exponential function can be expressed by the following equation:

$$I = A_1 \exp\left(\frac{-t}{\tau_1}\right) + A_2 \exp\left(\frac{-t}{\tau_2}\right) + C \quad (3)$$

where τ_i (i = 1, 2) is the decay lifetime. The fitting decay times are 2.5 and 21.3 ns corresponding to 6.5% and 93.5% of the total luminescence, respectively. The main component of 21.3 ns is a typical decay time in $Lu_{1-x}Sc_xBO_3$:Ce materials and can be compared with the result reported in the previous literature [18], while the cause of minor component 2.5 ns is still unclear. The effective lifetime (τ) is defined as [29]:

$$\tau = \frac{\int_0^\infty tI(t)dt}{\int_0^\infty I(t)dt} \quad (4)$$

The obtained effective lifetime of the Ce^{3+} ions is round 20.1 ns. Its decay time is very fast, so cerium-doped lutetium scandium orthoborate single crystal could be a potential scintillator for X-ray or γ-ray detection. The research on the growth and scintillation properties of $Lu_{1-x}Sc_xBO_3$:Ce crystals are worthy to be carried out further.

4. Conclusions

The influence of Sc/Lu on the phase transformation and luminescence was investigated by X-ray diffraction, photoluminescence, X-ray excited luminescence. The main conclusions are summarized as follows:

(1) It was found that the calcite phase of $LuBO_3$ can be stabilized up to 1550 °C when the n(Sc)/n(Lu + Sc) ratio is ≥10 at.%, at least. Furthermore, with the increase of the ratio from 10 at.% to 90 at.%, red shifts of Ce^{3+} emission wavelength are observed due to variation of Ce^{3+} crystallographic environment and the $4f^05d^1 \rightarrow 4f^1(^2F_{7/2})$ transition rate increases. In addition, with the increase of Ce^{3+} content from 0.1 at.% to 3 at.%, the self-absorption and nonradiative energy transfer from the host excitations (STE) to Ce^{3+} both play roles on the Ce^{3+} luminescence.

(2) $(Lu_{0.5}Sc_{0.5})_{0.995}Ce_{0.005}BO_3$ crystal was successfully obtained by Czochralski method. Its X-ray excited luminescence intensity can reach about 27% of LYSO:Ce scintilation crystal and its effective lifetime is round 20.1 ns. Hence, cerium-doped lutetium scandium orthoborate single crystal could be a potential scintillator in X-ray detection technology or γ-ray detection with improving the composition and crystal quality.

Acknowledgements

This work was supported by the National Natural Science Foundation of China (Grant No. 50902145), the Natural Science Foundation of Shanghai (Grant No. 09ZR1435800), and the Knowledge Innovation Program of the Chinese Academy of Sciences (Grant No. SCX200701).

References

[1] G.H. Ren, X.F. Chen, Y. Pei, H.Y. Li, H.X. Xu, J. Alloys Compd. 467 (2009) 120–123.
[2] P.S. Yu, A.H. Wu, L.B. Su, X. Guo, Y.B. Wang, H.Y. Zhao, Y. Yang, Q.H. Yang, J. Xu, J. Alloys Compd. 503 (2010) 380–383.
[3] D.H. Cao, G.J. Zhao, J.Y. Chen, Q. Dong, Y.C. Ding, Y. Cheng, J. Alloys Compd. 489 (2010) 515–518.
[4] F. Yang, S.K. Pan, D.Z. Ding, X.F. Chen, S. Lu, W.D. Zhang, G.H. Ren, J. Alloys Compd. 484 (2009) 837–840.
[5] F.A. Danevich, D.M. Chernyak, A.M. Dubovik, B.V. Grinyov, S. Henry, H. Kraus, V.M. Kudovbenko, V.B. Mikhailik, L.L. Nagornaya, R.B. Podviyanuk, O.G. Polischuk, I.A. Tupitsyna, Yu.Ya. Vostretsov, Nucl. Instrum. Methods Phys. Res. A 608 (2009) 107–115.
[6] H. Feng, D.Z. Ding, H.Y. Li, S. Lu, S.K. Pan, X.F. Chen, G.H. Ren, J. Alloys Compd. 489 (2010) 645–649.
[7] O. Sidletskiy, V. Baumer, I. Gerasymov, B. Grinyov, K. Katrunov, N. Starzhinsky, O. Tarasenko, V. Tarasov, S. Tkachenko, O. Voloshina, O. Zelenskaya, Radiat. Meas. 45 (2010) 365–368.
[8] M.J. Weber, S.E. Derenzo, C. Dujardin, W.W. Moses, Proceedings of the International Conference on Inorganic Scintillators and Their Applications, September, 1995, pp. 325–328.
[9] W.W. Moses, M.J. Weber, S.E. Derenzo, D. Perry, P. Berdahl, Proceedings of the International Conference on Inorganic Scintillators and Their Applications, September, 1997, pp. 22–25.
[10] L. Zhang, C. Pedrini, C. Madej, C. Dujardin, J.C. Ga^con, B. Moine, I. Kamenskikh, A. Belsky, D.A. Shaw, M.A. MacDonald, P. Mesnard, C. Fouassier, J.C. Van't Spijker, C.E.W. Van Eijk, Radiat. Eff. Defects Solids 150 (1–4) (1999) 47–52.
[11] D. Boyer, F. Leroux, G. Bertrand, R. Mahiou, J. Non-Cryst. 306 (2002) 110–119.
[12] G. Chadeyron-Bertrand, D. Boyer, C. Dujardin, C. Mansuy, R. Mahiou, Nucl. Instrum. Methods Phys. Res. B 229 (2005) 232–239.
[13] C. Mansuy, E. Tomasell, R. Mahiou, L. Gengembre, J. Grimblot, J.M. Nedelec, Thin Solid Films 515 (2006) 666–669.
[14] C. Mansuy, J.M. Nedelec, R. Mahiou, J. Mater. Chem. 14 (2004) 3274–3280.
[15] J. Yang, C.X. Li, X.M. Zhang, Z.W. Quan, C.M. Zhang, H.Y. Li, J. Lin, Chem. Eur. J. 14 (2008) 4336–4345.
[16] E. Levin, R.S. Roth, J.B. Martin, Am. Miner. 46 (1961) 1030–1055.
[17] J.-M. Nedelec, L. Courtheoux, E. Jallot, C. Kinowski, J. Lao, P. Laquerriere, C. Mansuy, G. Renaudin, S. Turrell, J. Sol–Gel Sci. Technol. 46 (2008) 259–271.
[18] S. Hatamoto, T. Yamazaki, J. Hasegawa, M. Katsurayam, M. Oshika, Y. Anzai, J. Cryst. Growth 311 (2009) 530–533.
[19] L. Pauling, J. Am. Chem. Soc. 51 (1929) 1010–1026.
[20] D.Z. Ding, S. Lu, L.S. Qin, G.H. Ren, Nucl. Instrum. Methods Phys. Res. A 572 (2007) 1042–1046.
[21] D.A. Keszler, H. Sun, Acta Cryst. C 44 (1988) 1505–1507.
[22] E.M. Levin, J. Am. Ceram. Soc. 50 (1967) 53–54.
[23] P. Dorenbos, Phys. Rev. B 62 (2000) 15640–15649.
[24] P. Dorenbos, Phy. Rev. B 64 (125117) (2001) 1–12.
[25] S.P. Feofilov, Y. Zhou, J.Y. Jeong, D.A. Keszler, R.S. Meltzer, J. Lumin. 125 (2007) 80–84.
[26] D.L. Dexter, J. Chem. Phys. 21 (1953) 836–850.
[27] A.R. Denton, N.W. Ashcroft, Phys. Rev. A 43 (1991) 3161–3164.
[28] K.T. Jacob, Shubhra Raj, L. Rannesh, Int. J. Mater. Res. 9 (2007) 776–779.
[29] Y.H. Zheng, H.P. You, G. Jia, K. Liu, Y.H. Song, M. Yang, H.J. Zhang, Cryst. Growth Des. 9 (2009) 5101–5107.